CrossMark

REGULAR PAPER

Mesoscale study of particle sedimentation with inertia effect using dissipative particle dynamics

**Hantao Liu · Shan Jiang · Zhen Chen · Moubin Liu ·
Jianzhong Chang · Yanhua Wang · Zhihui Tong**

Abstract Mesoscale dispersed two-phase flows often involve complicated dynamic behaviors. Grid-based methods within the framework of continuum mechanics are usually difficult to capture certain degree of molecular-level effect, while the molecular dynamics is only practical at extremely small temporal and spatial scales. In this paper, dissipative particle dynamics (DPD) is extended to the investigation of a fluid–solid sphere system with inertia effect within two parallel plates through the modification of DPD weighting function and hence the dynamic parameters. The sphere and walls are composed of frozen DPD particles that are first treated to reach equilibrium state in the simulation. The force on the solid sphere is obtained from all the particles included in the sphere. The drag coefficient of the frozen sphere is evaluated and compared with the classical correlations. The initial value problem for the sedimentation of the sphere is then solved at certain Reynolds numbers, which is consistent with our direct numerical simulation results.

H. Liu · J. Chang · Y. Wang · Z. Tong
Laboratory of Energy and Environment and Computational Fluid Dynamics, North University of China, Taiyuan 030051, China

H. Liu · S. Jiang · Z. Chen (✉)
Department of Civil and Environmental Engineering, University of Missouri, Columbia, MO 65211, USA
e-mail: liuhan@missouri.edu

S. Jiang
Department of Chemistry, University of Missouri, Columbia, MO 65211, USA

Z. Chen
Department of Engineering Mechanics, Dalian University of Technology, Dalian 116024, China

M. Liu
Chinese Academy of Sciences, Beijing 100190, China

1 Introduction

Particle motion and particle collision in the mesoscale channel are typical fluid–solid two-phase problems, which play an important role in the performance of many industrial processes involving suspension flows (Liu and Chang 2013). Analytical theories with simplified assumptions and experimental approaches with semi-empirical formulas are usually difficult to describe the forces acting on particles, the momentum transfer of fluid–solid system and the change of inter-phase boundary (Giacoma et al. 2014; Marco and Dimitris 2011; among others).

To investigate the inherent mechanism of mesoscale multiphase flows, many numerical methods have been developed, such as smoothed particle hydrodynamics (SPH; Liu and Liu 2003), lattice Boltzmann method (LBM; Shan and Chen 1993), direct simulation Monte Carlo (DSMC; Bird 1963) and true direct numerical simulation (TDNS; Feng and Joseph 1995), among which the most significant approach is TDNS that fully resolves the flow field around the particle and makes a direct coupling between the particle and fluid motion. Some interesting features have been reported, such as vortex shedding, particle trajectory, and the drafting, kissing and tumbling (DKT) scenario between two particles. In the TDNS, the fluid motion is governed by the traditional continuum-level Navier–Stokes equations. However, some molecular-level factors which are not fully considered in the TDNS may also play an important role at mesoscale.

Dissipative particle dynamics (DPD) was derived from Molecular Dynamics (MD), via coarse-graining the

molecular details to capture the physics at mesoscale, by Hoogerbrugge and Koelman (1992). It has been developed to simulate complex fluid flows involving colloidal suspension, polymer, phase separation, interface dynamics, membrane and two-phase flow at the mesoscopic scale (Liu et al. 2007; Revemga et al. 1999; Fan et al. 2006; among others). DPD is more computationally efficient than MD, and more sufficient to capture the details at mesoscale level than conventional continuum-level simulation techniques (Marsh et al. 1997). Hoogerbrugge and Koelman (1992) first studied the creep flow through a square array of cylinders and proved the possibility of using DPD to simulate hydrodynamic phenomena, in which the fluid flow was limited to creep flow and the inertia effect could be neglected. Boek et al. (1997) later computed the viscosity of suspended ball, pole and disk. With the modified DPD method proposed by Espanol and Warren (1995) and Boek and Schoot (1998) further investigated the fluid flow through periodic cylinder array and obtained the dimensionless drag force, which offers the feasibility of DPD simulation at certain limited Reynolds numbers. After that, Chen et al. (2006), and Kim and Philips (2004) computed the fluid flow through a sphere/cylinder. Their simulation results have shown that it is possible to simulate hydrodynamic phenomena at certain Reynolds numbers, but that it might be inaccurate at high Reynolds numbers because of the fluid compressibility.

In the DPD methods as summarized above, the DPD particles are treated to simulate the water response, but the dynamic properties of the DPD system, such as the Schmidt number, S_c, and its viscosity η, are far below those of water. In addition, there is no experimental or analytical solution to verify the typical sphere settlement in DPD simulation. In this paper, an improved DPD method is proposed that aims to study the fluid–solid system response at mesoscale, by resolving the water flow around a solid sphere and computing the particle force from the coupling between the solid and fluid particles. To validate the way how the solid sphere is represented in the simulation procedure, the numerical results are compared with the experimental correlations and direct numerical simulation (DNS) results.

2 DPD formulation

DPD simulates the motion of a set of interacting "particles". The particles move according to Newton's second law as follows:

$$\frac{d\mathbf{r}_i}{dt} = \mathbf{v}_i, \quad \frac{d\mathbf{v}_i}{dt} = \sum_j \mathbf{f}_{ij}, \tag{1}$$

where, $\mathbf{r}_i$ and $\mathbf{v}_i$ are the position and velocity vectors of the mass centre of particle i. The particle mass is taken as the unit of mass. The vector $\mathbf{f}_{ij}$ represents the interparticle force applied on particle i by particle j, which is assumed to be pairwise additive and consists of three parts, including a conservative force $\mathbf{F}_{ij}^C$, a dissipative force $\mathbf{F}_{ij}^D$ and a random force $\mathbf{F}_{ij}^R$, as shown below,

$$\mathbf{f}_{ij} = \mathbf{F}_{ij}^C + \mathbf{F}_{ij}^D + \mathbf{F}_{ij}^R, \tag{2}$$

In Eq. (1), the sum runs over for all other particles within a certain cutoff radius r_c, taken as the unit of length in the conventional DPD formulation. In the current study, it is allowed that $r_c \geq 1.0$, and its value varies for different kinds of forces. The cutoff radius will be further discussed in Sect. 3. The conservative force F_{ij}^c is a soft repulsion which is given by

$$\mathbf{F}_{ij}^C = \begin{cases} a_{ij}(1 - r_{ij})\hat{\mathbf{r}}_{ij}, & r_{ij} < r_c \\ 0, & r_{ij} \geq r_c \end{cases} \tag{3}$$

where a_{ij} is the maximum repulsion between particles i and j. $\mathbf{r}_{ij} = \mathbf{r}_i - \mathbf{r}_j$ with its amplitude $r_{ij} = |\mathbf{r}_{ij}|$, and $\hat{\mathbf{r}}_{ij} = \mathbf{r}_{ij}/r_{ij}$ is the unit vector directed from the mass centre of particle j to i. The dissipative and random forces take the forms of

$$\mathbf{F}_{ij}^D = -\gamma w^D(r_{ij})(\hat{\mathbf{r}}_{ij} \cdot \mathbf{v}_{ij})\hat{\mathbf{r}}_{ij}, \tag{4}$$

and

$$\mathbf{F}_{ij}^R = \sigma \zeta_{ij} w^R(r_{ij})\hat{\mathbf{r}}_{ij}, \tag{5}$$

respectively, where γ and σ are the coefficients characterizing the strengths of these forces. $w^D(r)$ and $w^R(r)$ are r-dependent weight functions vanishing for $r > r_c$. $\mathbf{v}_{ij} = \mathbf{v}_i - \mathbf{v}_j$, and ζ_{ij} is Wiener increment with the properties of

$$\langle \zeta(t)_{ij} \rangle = 0 \text{ and } \langle \zeta_{ik}(t)\zeta_{jl}(t') \rangle = (\delta_{ij}\delta_{kl} + \delta_{il}\delta_{jk})\delta(t - t'), \tag{6}$$

where $i \neq k$ and $j \neq l$. The detailed balance condition is similar to the Fluctuation–Dissipation theorem relating the strength of the random force to the mobility of a Brownian particle, which requires that

$$w^D(r) = \left[w^R(r)\right]^2 = \begin{cases} (1 - r/r_c)^s, & r < r_c \\ 0, & r \geq r_c \end{cases}$$
$$\gamma = \frac{\sigma^2}{2k_B T}, \tag{7}$$

with k_B being the Boltzmann constant, T the system temperature and s the exponent of the weighting function. In
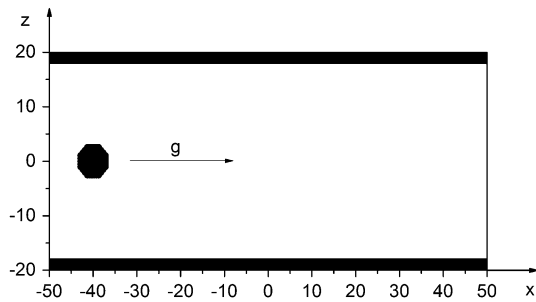
z

Fig. 1 Schematic diagram of the simulation domain

the traditional method, the s in the weight function for the dissipative force usually equals 2. Here, it is written in a more general form. The effect of s to the dynamic properties of the system will be discussed in Sect. 3.

Equation (7) ensures that the particulate temperature, strictly speaking, the fluctuation of the system kinetic energy, remains constant. As far as the thermal energy is concerned, the random two-particle force F_{ij}^R, which represents the results of thermal motion of all molecules contained in particles i and j, "heats up" the system. The dissipative force F_{ij}^D reduces the relative velocity of two particles and removes the kinetic energy from their mass center to "cool down" the system. When the detailed balance for Eq. (7) is satisfied, the system temperature will approach the given value. The dissipative and random forces act like a thermostat in the conventional MD system.

In the simulation, the DPD particles are frozen to simulate the solid object (sphere) and walls, as illustrated in Fig. 1. The solid object moves due to its gravity g as well as the interaction force from the surrounding fluid particles. The total force applied on the solid object is obtained via the summation looping through all the particles contained in the object. The differential equation governing the motion of the sphere mass center is given by

$$M\frac{\mathrm{d}V}{\mathrm{d}t} = G + F \tag{8}$$

where M is the total mass of the sphere, V is the velocity of the sphere, and G and F denote the body force of the sphere and the interactive force between the sphere and surrounding fluid particles, respectively. The differential equation governing the rotation of the sphere about its mass center takes the form of

$$\frac{\mathrm{d}(I\omega)}{\mathrm{d}t} = T \tag{9}$$

where T is the moment of external forces, I the mass moment of inertia, and ω the angular velocity.

3 Improved model parameters and test problems

3.1 Improved model parameters

In this section, parametric modification is conducted to improve the dynamic performance of the simulated DPD system. The proposed numerical scheme is then verified with the well-established experimental data and analytical solutions.

In the DPD simulation, the model parameters must be carefully chosen to describe the fluid as water. Groot and Warren (1997) found that to satisfy the compressibility of water, the coefficient of the conservative force should be

$$a_{ij} = 75k_BT/\rho \tag{10}$$

and recommended the values of $\sigma = 3.0$ and $\lambda = 0.65$ in the Verlet-type algorithm. In this paper, the density is chosen to be $\rho = 4.0$ so that the period of the face-centered-cubic (FCC) lattice becomes 1.0, and the plane lattice size of the solid sphere and wall particles is also equal to 1.0. The unit of energy is set to be k_BT, i.e., $k_BT = 1$. According to Eq. (7), we have $\gamma = 4.5$. It follows from Eq. (10) that $a_{ij} = a_{ff} = 18.75$ with the subscript f stands for "fluid." Until now, the study of the physical bases on how the solid particles interact to each other is still ongoing. In the current work, according to the research efforts from Fan et al. (Fan et al. 2003), it is assumed that $a_{ww} = 5.0$, where the subscript w stands for "wall or frozen," for the interaction between frozen particles, and that $a_{fw} = \sqrt{a_{ff}a_{ww}} = 9.6825$ for the interaction between fluid and frozen particles.

The dissipative force directly affects the rate of momentum transfer of the system and thus the dynamic properties of the system, such as the Schmidt number S_c and viscosity η. Since the Schmidt number of a typical DPD fluid, about 10^{-4} cP, is three orders of magnitude less than that of the water, various methods have been proposed to increase the dynamic properties, such as increasing the cutoff radius, decreasing the temperature, and/or increasing γ and using different thermostat for the system (Anurag et al. 2009; Low 1999; among others).

Similar to Groot and Warren's analysis (1997), assuming a uniform density ($g(r) \approx 1.0$), we can obtain the dynamic properties of the DPD system. The dissipative viscosity can be expressed as a function of s,

$$\eta^D = \frac{2\pi\gamma\rho^2}{15}\int_0^\infty r^4 w^D(r)\mathrm{d}r$$
$$= \frac{2\pi\gamma\rho^2 r_c^5}{15}\left(\frac{1}{s+1} - \frac{4}{s+2} + \frac{6}{s+3} - \frac{4}{s+4} + \frac{1}{s+5}\right) \tag{11}$$

As shown in Fig. 2 the dissipative viscosity decreases drastically with the increase of s. The dissipative viscosity can
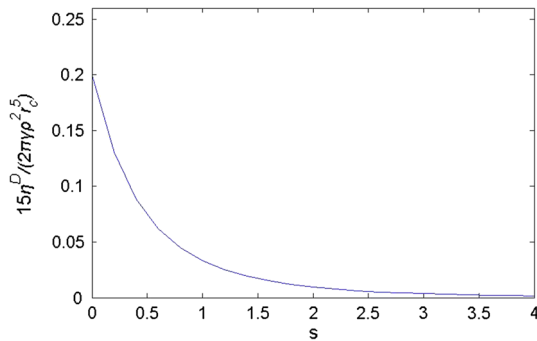
Fig. 2 The relationship between s and dissipative viscosity

be derived from the weight function of Eq. (7). When $s = 2$, the weight function for the conventional DPD formulation is recovered. The s is chosen on the premise that the continuity of the weighting function itself and a mild discontinuity of its gradient are satisfied, and it improves the dynamic properties of the DPD system such as the Schmidt number, S_c, and viscosity η. Hence $s = \frac{1}{2}$ is chosen in the present study.

Then, unlike the traditional weighting functions, $w^D(r) = (1 - r_c)^{1/2}$ is chosen in our simulation. $S_c = \frac{1}{2} + \frac{(2\pi\gamma\rho r_c^4)^2}{1999 k_B T}$ is also adopted in the current work, which becomes larger than $\frac{1}{2} + \frac{(2\pi\gamma\rho r_c^4)^2}{70875 k_B T}$ at $s = 2$. For example, if a set of parameters $\rho = 4$, $\gamma = 4.5$, $k_B T = 1.0$ and $r_c = 1.0$ are chosen, S_c would increase about ten times. It can be found from the above equation that S_c is proportional to γ^2 and r_c^8. To further increase the S_c, it is an efficient way to increase the values of γ and r_c. However, the increase of γ usually causes larger fluctuation of thermal energy, while the increase of r_c results in larger computation cost. Therefore, the weighting function used here is obtained by combining it with a moderate increase in the cutoff radius for the dissipative weighting function. Thus, S_c can reach to a certain level within a reasonable computational cost. With the moderate increase in the cutoff radius (in our current simulation $r_c = 2.0$), the values of diffusivity $D = 0.011$, viscosity $\eta = 71.288$ and Schmidt number $S_c = 1,636.907$ are chosen in the current work, respectively.

A modified version of the velocity-Verlet algorithm (Groot and Warren 1997) is used here, with the time step being 0.02. The flow domain is divided into grids, and local data are collected in each bin. The flow properties, such as stress, position, velocity, density and pressure, are calculated by averaging over all of the sampled data points in each bin over certain time steps.

3.2 Test problems

The Poiseuille flow in a slit is simulated first with the improved DPD formulation. The fluid domain is given by

$-30 \leq x \leq 30$, $-1.5 \leq y \leq 1.5$ and $-15 \leq z \leq 15$, respectively. The periodic boundary condition is applied in the x and y directions. The inner wall layers are located at $z = \pm 15.25$. There are 21,240 fluid particles in the channel and three wall layers parallel to the (x, y) plane consisting of 2,160 wall particles in each side. The dimensionless gravity ($g = 0.02$) is applied to each fluid particle at x direction, which later drives the flow.

The body force field is equivalent to imposing a pressure drop of $\rho g L_x$ in the channel with the length of L_x. The development of velocity profile at different time is illustrated in Fig. 3. It can be seen that the velocity profile is fully developed after about 1,200 time steps with a no-slip boundary condition. If the fluid is Newtonian, the analytical solution of Navier–stokes equation is

$$V_x = 3.75 \left[1 - \left(\frac{z}{15} \right)^2 \right] \tag{12}$$

As can be seen from Fig. 3, the analytical result is in a good agreement with the simulation data at $t = 1,200$.

In Fig. 4, the temperature with $k_B T = 1$ is uniformly across the channel. The density profile is also uniformly across the channel except for the regions near the walls, where small
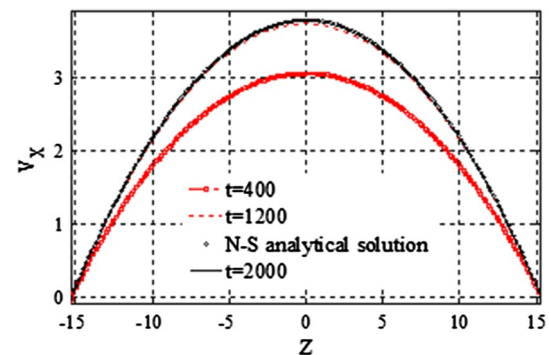

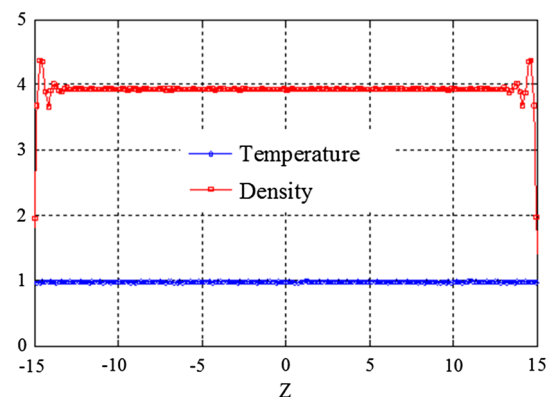**Fig. 3** The development of velocity profiles in Poiseuille flow

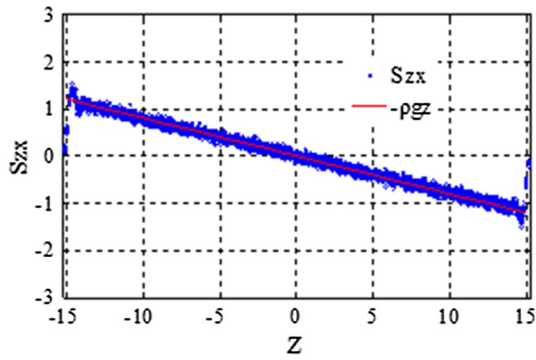**Fig. 4** The temperature and density profiles in Poiseuille flow

Fig. 5 The shear stress distribution in Poiseuille fluid

Fig. 6 The drag coefficient of a three dimensional spherical object at different Reynolds numbers

fluctuations in density still exist but are not as severe as those predicted by MD simulation (Kim et al. 2008).

The comparison of the shear stress predicted by DPD simulation with that obtained from the analytical solution is shown in Fig. 5. It can be seen that there is a very good agreement between two results across the channel, although there is some numerical noise in the regions near the wall surfaces.

4 Drag coefficient of a three dimensional sphere

To show the ability of the proposed procedure to deal with the problems relevant to inertia, the drag coefficient of a three dimensional sphere in the channel is considered here. The fluid domain is given by $-50 \leq x \leq 50$, $-8 \leq y \leq 8$ and $-20 \leq z \leq 20$, respectively. Periodic boundary condition is applied in the x and y directions. The inner wall layers are located at $z = \pm 20.25$. The center of sphere is located at $x = 0$, $y = 0$, $z = 0$ with its radius $r = 2.8$. There are 145,616 fluid particles in the channel, 12,000 particles in the walls parallel to the (x, y) plane in each side, and 384 frozen particles in the sphere, respectively. To achieve different Re numbers, the fluid particles are driven by different dimensionless gravity forces in the x-direction. The drag force is determined after the flow field is fully developed. Then the drag coefficient can be achieved from the equation as follow,

$$C_D = \frac{8 \times F_D}{\pi d^2 \rho_f U |U|} \tag{13}$$

where F_D is the drag force which is the summation of the interparticle force from all the particles included in the sphere, d is the diameter of the sphere, ρ_f is the fluid particle density, and U is the relative velocity between the sphere and the fluid along the x direction.

Figure 6 shows the results of the drag coefficient as compared with those from Batchelor's (1967), and Brown
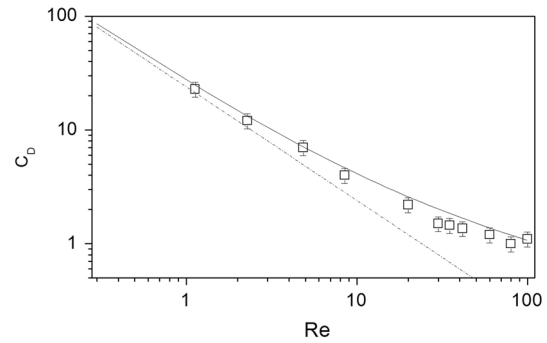
and Lawler's (2003) correlations. Batchelor's correlation is applicable to creeping flow, while the Brown's correlation is suitable for a broad extent with $Re \leq 2 \times 10^5$. It is shown that the DPD simulation results fit well with the correlations in the range of small Reynolds numbers and the difference between them increases with the increase of velocity.

5 Solid sphere sedimentation

Within the framework of conventional continuum mechanics, the behavior of a single sphere can be classified into five regimes: steady equilibrium with monotonic approach, steady equilibrium with a transient overshoot, weak oscillatory motion, strong oscillatory motion and irregular oscillatory motion, which occur at different Reynolds number intervals, depending on the channel width (Feng et al. 1994). While in DPD simulation, the reliable results are usually limited to the range of low Reynolds numbers, as discussed in Sect. 4 as well as other literatures (Chen et al. 2006; Kim and Phillips 2004; among others). Therefore, the sedimentation of a single DPD sphere is only simulated at low Reynolds number. A sphere that consists of 936 frozen DPD particles is released from the top of a channel with zero initial velocity, which moves according to Eqs. (8) and (9). The schematic diagram is shown in Fig. 1. The fluid domain of the channel is given by $-50 \leq x \leq 50$, $-1.5 \leq y \leq 1.5$ and $-20 \leq z \leq 20$, respectively, and filled with 47,400 fluid particles. The diameter of the sphere is 5.0. Periodic boundary condition is applied in the x and y directions. The inner wall layers are located at $z = \pm 20.25$. There are totally 3,600 frozen wall particles. The sphere is driven by the dimensionless gravity force in the x-direction. To compare the DPD results with the continuum hydrodynamics method, DNS, from our previous work (Chang et al. 2010), the channel width is set as the characteristic length, and the width and length are both set to be dimensionless.
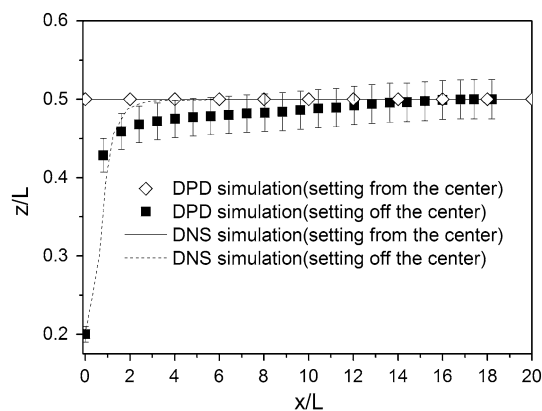
Fig. 7 Moving trajectories with the DPD and DNS solutions at $Re = 1.2$
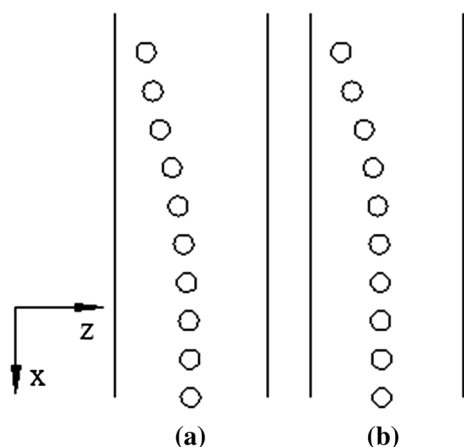

Fig. 8 Snapshots of DPD and DNS sphere distribution along the channel. **a** DPD sphere sedimentation; **b** DNS sphere sedimentation

The Reynolds numbers are determined by the terminal velocity. To get the same Reynolds number, the DPD sphere is subjected to a gravitational force, which equals to 0.03, and the ratio of DNS sphere to fluid is 1.00008 to 1.

The sphere trajectories are illustrated in Fig. 7. If it is released from the channel center, the DPD sphere will settle along the centerline and the sedimentation is stable, which is consistent with the result from our DNS simulation. If the sphere is released off the center, it will migrate to the centerline and eventually settle steadily along the centerline, which demonstrates the same trend as the DNS result but with a longer time to reach the center. This difference indicates that the DPD method, which can capture certain degree of molecular-level details, shows different sedimentary behavior from the DNS method which could only conform to the continuum hydrodynamics at larger length scales. The reason might be due to the fact that DPD method is a coarse-grained method, and the DPD fluid

particle may show a different performance of physical properties from the fluid in DNS. So it also implies that there is a scale effect on the sphere sedimentation by using the DPD and DNS methods. Besides, the understanding and formulation of the inherent relationship between the DPD particle and DNS fluid are still unknown for most cases. Figure 8 shows the detailed sphere distribution along the channel at different time instants in the DPD and DNS simulations, and demonstrates the difference we discussed above.

6 Concluding remarks and future tasks

A mesoscale simulation procedure is proposed in this paper to explore the fluid–solid system with the inertia effect by utilizing DPD simulation. First, the dynamic behavior of the DPD system is improved by modifying the traditional dissipative weighting functions. Then, the equations of motion for the frozen sphere are formulated based on rigid body dynamics. Finally, several typical cases are tested, and compared with the classical correlations or our DNS simulation results.

Within the parameter ranges examined, it is shown that the simulation results obtained from the improved DPD method are not only consistent with those from continuum hydrodynamics, but also could predict certain degree of molecular-level details, which indicates that the proposed procedure could become a useful numerical tool to study the behavior of mesoscale fluid–solid system with the inertia effect. Based on the preliminary results, the fluid–solid interaction problems with the inertia effect at a wider range of Reynolds numbers will be investigated in the future.

References

Anurag K, Yutaka A, Eiyad AN, Manfred K, Mohammad F (2009) From dissipative particle dynamics scales to physical scales: a coarse-graining study for water flow in microchannel. Microfluid Nanofluid 7:467–477

Batchelor GK (1967) An introduction to fluid dynamics. Cambridge University Press, Cambridge, pp 174–255

Bird GA (1963) Approach to translational equilibrium in a rigid sphere gas. Phys Fluids 6:1518–1519

Boek ES, Schoot HNWP (1998) Resolution effects in dissipative particle dynamics simulation. Int J Mod Phys C 9:1307–1318

Boek ES, Coveney PV, Schoot HNWP (1997) Simulating the rheology of dense colloidal suspensions using dissipative particle dynamics. Phys Rev E 55:3124–3133

Brown PP, Lawler DF (2003) Sphere drag and settling velocity revisited. J Environ Eng 129:222–228

Chang JZ, An K, Liu HT (2010) The study of the sedimentation of solid particle influenced by thermal convection using direct numerical simulation. Chin J Theor Appl Mech 42:205–211

Chen S, Phan-Thien N, Khoo BC, Fan XJ (2006) Flow around spheres by dissipative particle dynamics. Phys Fluids 18:103605–103605-14

Espanol P, Warren P (1995) Statistical mechanics of dissipative particle dynamics. Europhys Lett 30:191–196

Fan XJ, Phan-Thien N, Yong NT, Wu XH, Xu D (2003) Microchannel flow of a macromolecular suspension. Phys Fluids 15:11–20

Fan XJ, Phan-Thien N, Wu XH, Ng TY (2006) Simulation flow of DNA suspension using dissipative particle dynamics. Phys Fluids 18:063102

Feng J, Joseph DD (1995) The unsteady motion of solid bodies in creeping flows. J Fluid Mech 303:83–102

Feng J, Hu HH, Joseph DD (1994) Direct simulation of initial value problems for the motion of solid bodies in a Newtonian fluid Part 1. Sedimentation. J Fluid Mech 26:95–134

Giacoma A, Dureisseix D, Gravouil A, Rochette A (2014) A multiscale large time increment/FAS algorithm with time-space model reduction for frictional contact problems. Int J Mult Comp Eng 97:207–230

Groot RD, Warren PB (1997) Dissipative particle dynamics: bridging the gap between atomistic and mesoscopic simulation. J Chem Phys 107:4423–4435

Hoogerbrugge PJ, Koelman JMVA (1992) Simulating microscopic hydrodynamic phenomena with dissipative particle dynamics. Europhys Lett 19:155–160

Kim JM, Phillips RJ (2004) Dissipative particle dynamics simulation of flow around sphere and cylinders at finite Reynolds numbers. Chem Eng Sci 59:4155–4168

Kim BH, Beskok A, Cagin T (2008) Thermal interactions in nanoscale fluid flow: molecular dynamics simulations with solid-liquid interfaces. Microfluid Nanofluid 5:551–559

Liu HT, Chang JZ (2013) The implement and influence of different boundary conditions in direct simulation on particle sedimentation. Acta Phys Sin 62:084401

Liu GR, Liu MB (2003) Smoothed particle hydrodynamics—a mesh-free particle method. World Scientific, Singapore, pp 10–20

Liu MB, Meakin P, Huang H (2007) Dissipative particle dynamics simulation of fluid motion through an unsaturated fracture junction. J Comput Phys 222:110–130

Low CP (1999) An alternative approach to dissipative particle dynamics. Europhys Lett 47:145–151

Marco K, Dimitris D (2011) Multiscale simulation strategies and mesoscale modeling of gas and liquid flows. J Appl Math 76:661–671

Marsh CA, Backx G, Ernst XH (1997) Static and dynamic properties of dissipative particle dynamics. Phys Rev 56:1676–1691

Revemga M, Zuniga I, Espanol P (1999) Boundary conditions in dissipative particle dynamics. Comput Phys Commun 121:309–311

Shan XW, Chen HD (1993) Lattice Boltzmann model for simulating flows with multiple phases and components. Phys Rev 47:1815–1819